Journal of Animal and Feed Sciences, 33, 2, 2024, 170–184, https://doi.org/10.22358/jafs/175920/2024
The Kielanowski Institute of Animal Physiology and Nutrition, Polish Academy of Sciences, Jabłonna

Effect of feeding high fat diets differing in fatty acid composition **on oxidative stress markers and protein expression profiles** in mouse kidney

A. Wypych[1,*], **M. Ożgo**[1], M. Bernaciak[1], A. Herosimczyk[1], M. Barszcz[2], K. Gawin[2], A.K. Ciechanowicz[3], M. Kucia[3], **M. Pierzchała**[4], **E. Poławska**[4] **and A. Lepczyński**[1]

[1] West Pomeranian University of Technology, Faculty of Biotechnology and Animal Husbandry, Department of Physiology, Cytobiology and Proteomics, Szczecin 71-270, Poland
[2] The Kielanowski Institute of Animal Physiology and Nutrition, Polish Academy of Sciences, Department of Animal Nutrition, 05-110 Jabłonna, Poland
[3] Medical University of Warsaw, Centre for Preclinical Research and Technology, Laboratory of Regenerative Medicine, 02-091 Warsaw, Poland
[4] Institute of Genetics and Animal Biotechnology of the Polish Academy of Sciences, Department of Genomics and Biodiversity, 05-552 Magdalenka, Poland

KEY WORDS: high-fat diet, kidney, omega-3, omega-6, proteome, saturated fats

Received: 27 October 2023
Revised: 24 November 2023
Accepted: 27 November 2023

* Corresponding author:
e-mail: agata.grzesiak@zut.edu.pl

ABSTRACT. High-fat diets (HFDs) are associated with the development of metabolic disorders. However, the type of dietary fat may also be a critical risk factor. The study aimed to determine the effect of three months of feeding HFDs with different fatty acid composition on oxidative stress markers and the proteome of mouse kidneys. The study involved 24 Swiss-Webster mice, which were divided into four groups (n = 6) fed for three months a standard chow (STD), an HFD rich in saturated fatty acids (SFA), and HFDs rich in polyunsaturated fatty acids with linoleic acid to α-linolenic acid ratios of 14:1 (HR) or 5:1 (LR). Feeding the SFA and HR diets increased triglyceride levels compared to the STD and LR groups. The HR group also had higher concentrations of thiobarbituric acid reactive substances compared to the other groups. There was no effect of HFD on cholesterol concentration and activity of antioxidant enzymes. The SFA diet increased the expression of acyl-CoA thioesterase 2 and D-lactate dehydrogenase, while decreasing that of apolipoprotein E. All HFDs led to downregulation of ATP synthase F1 subunit beta, mitochondrial, while only the LR diet increased the expression of persulphide dioxygenase ETHE1 and electron transfer flavoprotein subunit A, suggesting an enhanced oxidation of fatty acids. Ingestion of the SFA and HR diets caused downregulation of molecular chaperones and upregulation of the inflammation and apoptosis regulator peptidylprolyl isomerase A. In conclusion, feeding SFA and HR diets induces oxidative stress and proteome changes in the mouse kidney. The SFA diet most significantly influenced the expression pattern of proteins related to energetic metabolism.

Introduction

Excessive fat intake, particularly the consumption of high levels of saturated fatty acids (SFA), promotes adverse metabolic changes that contribute to the development of overweight and obesity (Wu et al., 2022). The latter condition has been shown to contribute to the development of chronic diseases, including chronic kidney disease (CKD). However, the complex links between obesity and CKD have not

been fully elucidated (Than et al., 2020). The molecular response of kidney cells to excess supply of dietary fatty acids, as in a high-fat diet (HFD), involves cellular uptake through known fatty acid transporters (Yang et al., 2017). This results in the modification of fatty acids (FA) metabolism in renal tubular cells, including impairments in FA β-oxidation, tricarboxylic acid cycle (TCA) and mitochondrial chain function, ultimately leading to reduced ATP synthesis (Szeto et al., 2016). The unmetabolised FA pool is converted into triglycerides and stored in epithelial cells in the form of lipid droplets (Tang et al., 2016). These perturbations in energetic metabolism induce oxidative stress, which requires the activation of stress-preventing mechanisms, such as reactive oxygen species (ROS) scavengers and molecular chaperones, to preserve cell function (Sun et al., 2020; Sánchez-Navarro et al., 2021). Moreover, prolonged stress related to increased fat intake, such as ectopic lipid accumulation and lipid peroxide production, may lead to the induction of an inflammatory response and activation of pathways involved in increased extracellular matrix deposition (Yang et al., 2017). These processes in turn can contribute to abnormalities in kidney microstructure, including thickening of the glomerular basement membrane, expansion of mesangial cells in the glomeruli, autophagy and/or apoptosis of glomerular vascular endothelial cells and tubular epithelial cells, as well as infiltration of inflammatory cells (Szeto et al., 2016).

Conversely, numerous studies have indicated that an increased intake of polyunsaturated fatty acids (PUFA) may exert reno-protective effects. For example, a large and comprehensive analysis that included the results of 19 cohort studies clearly demonstrated that n-3 PUFA derived from seafood might reduce the risk of CKD development (Ong et al., 2023). However, limited evidence suggests a protective role of n-6 PUFA on kidney function, particularly linked to the impact of improved lipid metabolism in elderly individuals (Syren et al., 2018). These observations are not surprising given the effects of active metabolites of PUFA. Eicosanoids derived from n-6 PUFA exhibit mainly pro-inflammatory effects, while those derived from n-3 PUFA have anti-inflammatory properties. Therefore, maintaining the proper dietary ratio of n-6 to n-3 PUFA (2-5:1) is crucial to increase the formation of active metabolites derived from n-3 PUFA (Liput et al., 2021). This finding was confirmed in a previous study that sought to assess the effect of high-fat diets (HFDs) rich in SFA or PUFA with high (14:1) and recommended (5:1) n-6 to n-3 ratios on kidney microstructure and the expression of stress-related genes. It was clearly demonstrated that animals fed an HFD rich in SFA and n-6 PUFA showed an increased vacuolisation of tubular epithelial cells, a higher incidence of tubular cell apoptosis and increased collagen deposition in the kidney interstitium. These pathophysiological lesions were accompanied by an increased expression of the *Kim1* gene, a marker of tubular cell damage. However, these adverse effects were ameliorated in animals fed an HFD with the highest n-3 PUFA content (Wypych et al., 2023).

The response of the kidney to metabolic disturbance caused by an HFD remains incompletely understood and still requires in-depth analysis. As outlined above, FA composition also has a significant impact on the modulation of the renal cell response to HFD, suggesting differential regulation of numerous metabolic and signalling pathways by this dietary factor. Such regulation leads to the substantial changes in gene/protein expression patterns. A comprehensive analysis of these changes in gene and protein expression necessitates the application of omics technique (Provenzano et al., 2022). Among these, proteomic analyses are powerful tools for studying the impact of multiple factors on kidney function (Ożgo et al., 2007). Recent work by Dozio et al. (2022) described significant changes in the expression of proteins involved in lipid metabolism, response to cellular stress, and profibrotic signalling pathways in mice subjected to an SFA-rich HFD. To our knowledge, data regarding the impact of PUFA-rich HFDs on the protein expression profile in the kidney are lacking.

Therefore, the objective of the present study was to determine the effects of a three-month feeding regimen with HFDs containing varying fatty acid (FA) compositions on both oxidative stress markers and the mouse kidney proteome.

Material and methods

Experiment design and animal housing

The experimental procedures were carried out in accordance with EU legislation and approved by the 2nd Warsaw Local Ethics Committee for Animal Experimentation (decision number WAW2_22/2016). The housing and feeding conditions were described in detail in previous applications by Lepczyński et al. (2021) and Wypych et al. (2023). Briefly, the experiment was conducted using 24 ten-week-old male Swiss-Webster mice divided into four groups fed for three months with standard (STD) chow (Labofed H, Morawski Feed

Production Plant, Kcynia, Poland), an HFD rich in SFA, and an HFD rich in PUFA with linoleic acid (LA) to α-linolenic acid (ALA) ratios of 14:1 (high ratio, HR) or 5:1 (low ratio, LR). The animals were housed in a controlled environment with a 12-h dark/light cycle. During the experiment, animals had free access to water and were fed *ad libitum* twice daily to avoid FA oxidation. Different qualitative FA compositions were obtained by supplementing the standard diet with appropriate plant oils. Ingredient and chemical composition of diets are given in Table 1. At the end of the trial, animals were fasted overnight (12 h) and weighed before euthanasia, performed using an UNO Euthanasia Unit (Uno Roestvaststaal BV, Zevenaar, Netherlands). Following this step, the kidneys were immediately collected and snap-frozen in liquid nitrogen.

Table 1. Ingredient and chemical composition of diets for mice

Item	Groups			
	STD	SFA	HR	LR
Ingredients, g/kg				
Labofeed H*	1000	790	790	790
virgin coconut oil	–	200	–	20
pumpkin seed oil	–	10	210	65
sunflower seed oil	–	–	–	80
avocado oil	–	–	–	20
hemp seed oil	–	–	–	15
maize oil	–	–	–	10
Chemical composition, %				
crude protein	22.0	17.4	17.4	17.4
crude fat	4.2	24.3	24.3	24.3
crude fibre	3.5	2.8	2.8	2.8
crude ash	5.7	4.5	4.5	4.5
SFA%	24.85	76.87	1.68	9.91
PUFA%	12.27	11.04	82.21	79.69
MUFA%	62.88	12.09	16.10	10.40
LA/ALA	1.57	1.41	13.76	5.00

STD – group fed a standard diet, SFA – group fed a diet rich in saturated fatty acids, HR – group fed a diet rich in polyunsaturated fatty acids with high ratio of linoleic acid to α-linolenic acid, LR – group fed a diet with low ratio of linoleic acid to α-linolenic acid; * Labofeed H contained: grains and grain by-products, soybean meal, flaxseed meal, yeasts, potato protein, dried whey, minerals and vitamins; SFA – saturated fatty acids, PUFA – polyunsaturated fatty acids, MUFA – monounsaturated fatty acids, LA/ALA – linoleic acid (18:2 n-6) to α-linolenic acid (18:3 n-3) ratio

Biochemical analyses

Blood for biochemical analyses was collected by post-mortem cardiac puncture and collected into tubes coated with lithium heparin (determination of Na, Cl, K, Mg, P, and creatinine concentrations) or NaF/K_3EDTA (lactate concentration analysis). Subsequently, blood samples were centrifuged (3000 *g*, 10 min, 4 °C) and blood plasma was collected. Biochemical analyses of blood plasma were performed using a COBAS INTEGRA® 400 plus system (Roche Diagnostics Ltd., Rotkreuz, Switzerland) and dedicated COBAS diagnostics tests.

For renal biochemical analyses, one kidney from each mouse was homogenised in 1 ml of ice-cold 0.9% NaCl at high speed and centrifuged (10000 *g*, 10 min, 4 °C). Cholesterol and triglyceride concentrations were measured in the supernatant using a MAXMAT PL analyzer (Erba Diagnostics France SARL, Montpellier, France) and ELITech Clinical Systems SAS (Sees, France) diagnostic kits.

The concentration of thiobarbituric acid-reactive substances (TBARS), a marker of lipid peroxidation, was analysed photometrically as described by Chodkowska et al. (2022). Absorbance was measured using a SpectraMax iD3 multi-mode microplate reader (Molecular Devices, LLC., San Jose, CA, USA) set at 532 nm. TBARS concentration was calculated using a standard curve for malonyldialdehyde.

Renal catalase (CAT) and glutathione peroxidase activities were measured spectrophotometrically using the Catalase Assay Kit (Megazyme, Bray, Ireland) and Glutathione Peroxidase (GSH-PX) Assay Kit (BT LAB, Shanghai, China), respectively, according to the manufacturers' instructions. After enzymatic and colour reactions, the solutions were transferred to a 96-well microplate and absorbance was measured at 520 nm for catalase and 412 nm for glutathione peroxidase using a SpectraMax iD3 reader (Molecular Devices, LLC., San Jose, CA, USA).

Total superoxide dismutase (SOD) activity was measured in samples transferred to a 96-well microplate, following the modified method of Marklund and Marklund (1974) based on the enzyme's ability to inhibit autooxidation of pyrogallol at alkaline pH. To each well, 2 µl of kidney supernatant and 248 µl of Tris-HCl buffer (50 mM, pH 8.2) containing 1 mM diethylenetriaminepentaacetic acid (DTPA) were added and pre-incubated for 4 min at 25 °C in a SpectraMax iD3 microplate reader (Molecular Devices, LLC., San Jose, CA, USA). Subsequently, 10 µl of 5 mM pyrogallol (in 10 mM HCl) were added, and the microplate was shaken for 15 s at medium speed. The blank contained 0.9% NaCl instead of a sample, Tris-HCl-DTPA buffer and pyrogallol. Using the kinetic mode of the reader, absorbance was measured at 420 nm for 4 min at 60-s intervals. The reading chamber's temperature was maintained

at 25 °C throughout the measurement. After the reading, the increase in absorbance per minute was calculated for each sample and then, the inhibition of the reaction was determined in relation to the blank considered as 100%. The samples were diluted to obtain the inhibition in a range of 15–65%. Total SOD activity was differentiated into CuZn SOD (SOD-1, cellular) and Mn SOD (SOD-2, mitochondrial) activities using Tris-HCl-DTPA buffer with 1 mM KCN, which inhibits CuZn SOD. After the reaction set for Mn SOD and performed under the same conditions, CuZn SOD activity was calculated as the difference between total and Mn SOD activities.

Total protein concentration in kidney supernatants was determined spectrophotometrically by the Bradford method using the Bio-Rad Protein Assay Kit II (Bio-Rad, Hercules, CA, USA).

Protein sample preparation

Kidney samples were pulverised in a mortar in the presence of liquid nitrogen. The tissue powder was then homogenised in a lysis buffer (7 M urea, 2 M thiourea, 4% w/v, 1% w/v DTT, 2% v/v Biolyte, 1% v/v protease inhibitor cocktail) using a steel ball homogeniser (Tissue Lyser, Qiagen, Hilden, Germany) for 30 min (22 Hz). Next, insoluble tissue debris was sedimented by centrifugation (22000 *g*, 20 min, 0 ºC) and the supernatant was collected and used as a protein sample for 2-DE.

Two-dimensional electrophoresis (2-DE)

The total protein concentration in the kidney protein samples was determined using a modified Bradford assay (Protein Assay Dye Reagent Concentrate, Bio-Rad, Hercules, CA, USA). Protein samples containing 450 μg of total protein, in 250 μl of lysis buffer (5 M urea, 2 M thiourea, 4% CHAPS, 1% (w/v) dithiothreitol (DTT), 0.5% (v/v) carrier ampholytes) were subjected to isoelectric focusing (IEF). Prior IEF, samples were loaded onto 11 cm IPG strips with a non-linear 3–10 pH gradient through a two-step rehydration process (passive – 5 h, 0 V and active – 12 h, 50 V). Subsequently, IEF was run in a Protean i12 IEF Cell (Bio-Rad, Hercules, CA, USA) using the following program: 250 V for 125 Vh, 500 V for 250 Vh, 1000 V for 500 Vh in rapid mode, linear voltage increase to 3500 V over one and a half hours, 3500 V for 35000 Vh in rapid mode (total IEF 37 kVh).

After IEF, IPG strips were incubated for 15 min in an equilibration buffer (6 M urea, 0.5 M Tris/HCl, pH 6.8, 2% w/v SDS, 30% w/v glycerol) with 1% DTT addition. The strips were then washed for 20 min in an equilibration buffer with 2.5% iodoacetamide. Two-dimensional electrophoresis was run in 12% polyacrylamide gels in a Protean Plus™ Dodeca Cell™ electrophoretic chamber (Bio-Rad, Hercules, CA, USA) using the following parameters: 40 V for 2.5 h, followed by 100 V for 16 h (15 °C). Protein samples were run simultaneously with Precision Plus Protein™ Standard Plugs (Bio-Rad, Hercules, CA, USA) as a reference.

Gel staining and image acquisition

After 2-DE separation, proteins in the gels were detected using CBB G-250, as described by Lepczyński et al. (2021). The gels were first washed twice in ddH_2O for 5 min. Subsequently, the proteins in the gels were fixed using a buffer containing 50% ethanol, and 5% phosphoric acid in ddH_2O (3 h). Then, the gels were stained for 3 h in Bradford solution (Bio-Rad Protein Assay, Bio-Rad, Hercules, CA, USA) diluted 1:19 in ddH_2O. After staining, the gels were washed with ddH_2O (3 times; 15 min). Digital gel images were acquired using a GS-800™ Calibrated Densitometer (Bio-Rad, Hercules, CA, USA).

Gel image densitometric analysis

Densitometric analysis of digital gel images was conducted using PDQuest 8.0.1 advanced software (Bio-Rad, Hercules, CA, USA). The spots present on all gels, representing each group, were considered as expressed protein spots and were included in analysis. Spot volume was estimated as the parameter used to quantify protein spots. A local regression model was used for data normalisation. Significance of differences between the control and each experimental group was calculated using Student's t-test ($P \leq 0.05$) through the integrated statistical tool. To assess within-group variability, the coefficient of variation (CV) was calculated. The experimental isoelectric point (pI) and molecular weight (kDa) values were determined for each identified significantly altered protein spot.

MALDI-ToF mass spectrometry protein identification

Reproducible protein spots showing statistically significant alterations between the STD and experimental groups were selected for identification. These protein spots were excised from the gels and processed as previously described by Ożgo et al. (2015). Protein identification was conducted using a MALDI FT-ICR mass spectrometer (SolariX 2xR, Bruker Daltonics, Bremen, Germany), following the procedure detailed by Herosimczyk et al. (2022).

The identification process employed MALDI as an ionization method, with a smartbeam™ II 1 kHz using a 355 nm solid state Nd:YAG laser focused to a diameter of ~25 μm as an energy source. Mass spectra were collected in the positive mode using 1000 laser shots from each spot. Internal mass calibration was performed using a lock mass calibration on a known m/z and an external sodium formic acid cluster calibrant. Data acquisition was performed using ftControl, and subsequent analysis was conducted using Data Analysis software (Bruker Daltonics, Bremen, Germany).

Peptide mass fingerprinting (PMF) data were compared with vertebrate databases (SWISS-PROT; http://us.expasy.org/uniprot/, accessed 19 October 2020 and NCBI http://www.ncbi.nlm.nih.gov/, accessed 19 October 2020) using the MASCOT search engine (http://www.matrixscience.com/) implemented in Protein Scape 4.2 software (Bruker Daltonics, Bremen, Germany). Search criteria included trypsin as the enzyme, carbamidomethylation as the fixed modification, and deamidation (NQ), oxidation (M) and Gln→pyro-Glu (N-term Q) as variable modifications of the SolariX 2xR MRMS data. Peptide mass tolerance ranged from 50 to 150 ppm, with a maximum of two missed cleavage sites. A custom-made contaminant list was applied to clean the peak list of the samples. The results of PMF-based identification were accepted when the protein score was significant ($P < 0.05$) with at least 9 matching peptides and 15% sequence coverage.

Gene Ontology (GO) analysis

GO enrichment analysis and protein-protein interactions (PPI) of significantly altered gene expression products were performed using the web-based STRING v11.5 software (Szklarczyk et al., 2023), with the murine genome as the background. The following interaction search options were selected: interaction score of 0.400 (medium confidence) and identification of significant results based on the Benjamini-Hochberg False Discovery Rate set at $P < 0.05$. Functional association was established based on the STRING cluster enrichment results.

Statistical analysis

Blood and renal biochemical parameters were analysed using one-way analysis of variance followed by Duncan's *post hoc* test. All statistical analyses were conducted using Statgraphics Centurion XVI ver. 16.1.03 (StatPoint Technologies, Inc. Warrenton, VA, USA), with the significance level set at $P \leq 0.05$).

Results

Morphometric differences

Feeding an HFD affected body weight gain and relative kidney weight of mice. Additionally, SFA and HR diets caused significant pathophysiological changes in the kidneys, such as increased tubular vacuolisation, collagen deposition and increased TUNEL staining, indicating apoptosis. These observations have been previously described and discussed by Wypych et al. (2023).

Biochemical parameters

The biochemical parameters of blood plasma and kidneys of mice are presented in Table 2. The concentrations of Na, K, P, Mg, creatinine, and lactate did not differ between the groups, but feeding an HFD significantly reduced blood Cl levels ($P = 0.0022$). Moreover, the study observed a significant increase in kidney triglyceride concentration when mice were fed SFA and HR diets ($P = 0.0124$) compared to the STD and LR groups. Additionally, the HR group displayed a higher ($P = 0.0351$) TBARS concentration in comparison to the other groups. Notably, there was no effect of the HFD on total cholesterol levels and antioxidant enzyme activities in mouse kidneys.

Differences in protein expression profile induced by HFD

The coefficient of variation (CV) for the STD, SFA, HR and LR groups was estimated at 64.22%, 60.74% and 60.22%, respectively. A comparative densitometric analysis was performed for 179 protein spots present on each gel, representing renal proteome profiles. This analysis revealed significant differences between the control group and the groups fed individual HFDs. In total, 23 successfully identified protein spots representing the expression products of 19 individual genes were found to be differentially regulated in response to the experimental diets compared to the STD group. Administration of the SFA diet induced differences in the expression of 11 identified proteins. Of these, 7 were upregulated (peroxiredoxin-6 (PRDX6), peroxiredoxin-1 (PRDX1), peptidyl-prolyl cis-trans isomerase A (PPIA), probable D-lactate dehydrogenase (LDHD), acyl-coenzyme A thioesterase 2 (ACOT2), 3-hydroxyisobutyrate dehydrogenase (HIBADH), methylmalonate-semialdehyde/malonate-semialdehyde dehydrogenase [acylating] (ALDH6A1)), while 4 were downregulated (60 kDa heat shock protein (HSPD1), apolipoprotein E (Apo-E),

Table 2. Biochemical indices in blood plasma and kidneys after three-months of feeding of standard mouse diet (STD) and experimental high-fat diets

Blood plasma	Groups				SEM	*P*-value
	STD	SFA	HR	LR		
Na, mmol/l	168.90	170.99	165.45	168.06	1.088	0.3540
K, mmol/l	8.80	6.78	9.09	7.96	0.439	0.2474
Cl, mmol/l	111.40^{b}	106.51^{a}	108.32^{a}	107.94^{a}	0.497	0.0022
P, mmol/l	3.05	3.21	3.00	3.09	0.076	0.7974
Mg, mmol/l	0.11	0.11	0.15	0.11	0.009	0.2924
Creatinine, µmol/l	8.68	7.62	7.06	8.78	0.358	0.2568
Lactate, mmol/l	9.71	12.30	12.69	10.39	0.489	0.0800
Kidney						
cholesterol, µmol/g	7.25	8.66	7.56	8.15	0.274	0.3049
triglycerides, µmol/g	5.65^{a}	9.69^{b}	8.95^{b}	5.40^{a}	0.636	0.0124
TBARS, µmol/g	19.39^{a}	27.88^{ab}	47.17^{b}	19.88^{a}	4.278	0.0351
GSH-PX, U/mg protein	11.01	9.40	10.39	11.49	0.956	0.9099
catalase, U/mg protein	105.5	177.0	145.8	141.5	10.46	0.1265
total SOD, U/mg protein	28.26	25.15	23.82	23.60	1.046	0.4115
Mn SOD, U/mg protein	12.13	12.53	10.19	11.49	1.034	0.8773
CuZn SOD, U/mg protein	16.14	12.62	13.63	12.11	1.284	0.7511

SFA – group fed a diet rich in saturated fatty acids, HR – group fed a diet rich in polyunsaturated fatty acids with a high ratio (14:1) of linoleic acid to α-linolenic acid, LR – group fed a diet with a low ratio (5:1) of linoleic acid to α-linolenic acid, TBARS – thiobarbituric acid-reactive substances, GSH-PX – glutathione peroxidase, SOD – superoxide dismutase, SEM – standard error of the mean; ^{ab} - means within a row with different superscripts are significantly different; $P < 0.05$ indicates that the data are significantly different

isocitrate dehydrogenase [NADP] cytoplasmic (IDH1), ATP synthase subunit beta (ATP5F1B)). In the HR group, seven proteins were found to be differentially expressed in the kidney, with 4 showing downregulation (endoplasmic reticulum chaperone BiP (HSPA5), PRDX6, ATP5F1B, ALDH6A1) and 3 upregulation (PPIA, aldo-keto reductase family 1 member A1 (AKR1A1), isocitrate dehydrogenase [NADP], mitochondrial (IDH2)). Twelve proteins were differentially regulated in the kidney of animals fed the LR diet, with 9 being upregulated (PRDX1, protein disulfide-isomerase (P4HB), AKR1A1, alpha-enolase (ENO1), persulfide dioxygenase ETHE1, mitochondrial (ETHE1), IDH1, electron transfer flavoprotein subunit alpha, mitochondrial (ETFA), ALDH6A1, 3-hydroxyanthranilate 3,4-dioxygenase (HAAO)) and 3 downregulated (IDH1, ATP5F1B). It should be emphasised that IDH1 protein was identified with multiple spots, among which, two were down- and one was upregulated in the LR group. A representative 2-D map of the murine renal proteome, along with the aforementioned differentially expressed proteins, is illustrated in Figure 1. Detailed data concerning the differences in protein expression and identification parameters of spots with varying intensities are presented in Table 3.

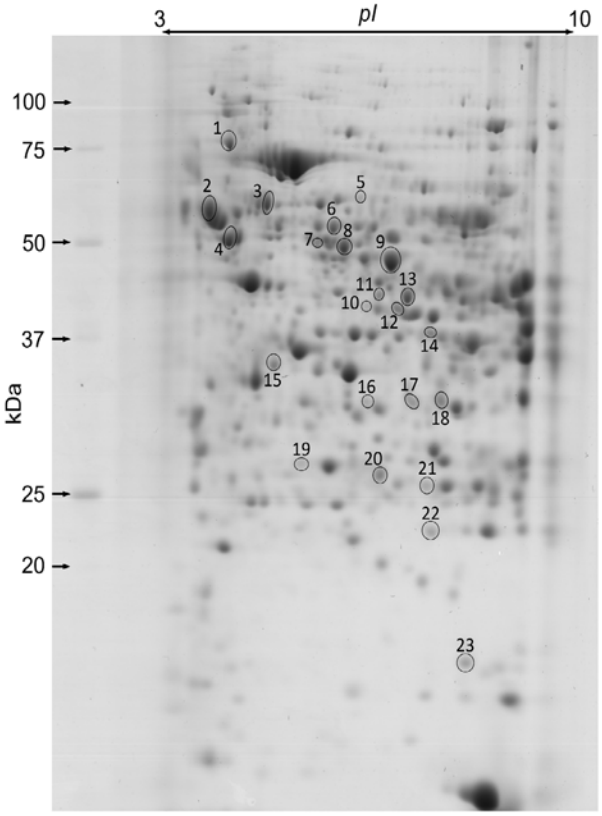

Figure 1. Representative two-dimensional gel electrophoresis image of the kidney protein profile. Numbers indicate differentially expressed ($P \leq 0.05$) proteins between the group fed a standard diet and the groups fed high-fat diets. Protein spot numbers refers to those shown in Table 3

Table 3. List of identified protein spots with different expression in mouse kidney in response to different high-fat diets

No.	Protein name	Gene name	Acc. no.	Seq. cov./M. score	STD	SFA	SFA / STD	HR	HR / STD	LR	LR / STD	Predicted pI/Mw	Estimated pI/Mw
	Stress response												
1	endoplasmic reticulum chaperone BiP	Hspa5	P20029	55%/93	240.1	195.6	0.81	156	0.65	202	0.84	5.07/72.49	4.7/77.0
3	60 kDa heat shock protein	Hspd1	P63038	85%/136	306	174.2	0.57	261.6	0.85	285.3	0.93	5.67/61.09	5.3/59.4
22	peroxiredoxin 1	Prdx1	P35700	68%/65	41.6	76.9	1.85	37.1	0.89	68.6	1.65	8.26 / 22.39	7.9/22.3
19	peroxiredoxin 6	Prdx6	O08709	81%/65	100	89.4	0.89	63.4	0.63	93.5	0.94	5.71/24.97	5.8/27.0
20	peroxiredoxin 6	Prdx6	O08709	87%/67	23.9	v45.8	1.92	22.1	0.92	22.3	0.93	5.71/24.97	7.1/26.2
2	protein-disulphide isomerase	P4hb	P04785	39%/136	452.6	538.4	1.19	505	1.12	637.4	1.41	4.82/57.31	4.3/58.8
	Inflammation and apoptosis												
23	peptidyl-prolyl cis-trans isomerase	Ppia	P17742	84%/63	67.1	110.2	1.64	127.6	1.9	99.2	1.48	7.74/18.13	8.5/15.2
	glycolysis/Gluconeogenesis												
14	aldo-keto reductase family 1 member A1	Akr1a1	Q9JII6	73%/76	27.7	44.3	1.6	48.9	1.76	66.5	2.4	6.90/36.79	7.9/37.7
9	alpha-enolase	Eno1	P17182	79%/117	446.8	481.8	1.08	444.5	0.99	556.9	1.25	6.37/47.45	7.3/47.0
8	probable D-lactate dehydrogenase	Ldhd	Q7TNG8	72%/109	208.9	370.3	1.77	260.5	1.25	259	1.24	6.15/52.50	6.5/49.5
	Lipid metabolism fatty acids β-oxidation												
5	acyl-coenzyme A thioesterase 2	Acot2	O55137	44%/76	12.8	28.1	2.19	15.8	1.23	22.2	1.73	6.12/46.34	6.8/60.9
21	persulphide dioxygenase ETHE1	Ethe1	Q9DCM0	81%/72	22.1	24	1.09	27.3	1.24	32.8	1.49	6.78/28.24	7.8/25.3
15	apolipoprotein E	Apoe	P02650	29%/61	177.9	104.1	0.59	160.8	0.9	170.2	0.96	5.23/35.79	5.4/34.7
	Tricarboxylic acid cycle												
11	isocitrate dehydrogenase [NADP] cytoplasmic	Idh1	O88844	75%/111	84	54.9	0.65	78.9	0.94	54.2	0.64	6.73/47.04	7.1/42.6
12	isocitrate dehydrogenase [NADP] cytoplasmic	Idh1	O88844	78%/70	46.6	77.2	1.66	65.5	1.41	89.6	1.93	6.73/47.04	7.4/40.8
10	isocitrate dehydrogenase [NADP] cytoplasmic	Idh1	O88844	88%/171	20.7	30.1	1.46	18.8	0.91	12.5	0.61	6.73/47.04	6.9/40.9
13	isocitrate dehydrogenase [NADP], mitochondrial	Idh2	P54071	79%/111	139.7	108.1	0.77	199.1	1.42	161.5	1.16	6.48/47.03	7.5/42.2
	Respiratory chain-associated proteins												
18	electron transfer flavoprotein subunit alpha	Etfa	Q99LC5	77%/73	54.8	78.9	1.44	73.8	1.35	99.7	1.82	8.62/35.33	8.1/31.6
4	ATP synthase subunit beta	Atp5f1b	P56480	89%/138	528.8	428.3	0.81	304.9	0.58	383.2	0.72	5.19/56.27	4.7/50.7
	Amino acids metabolism												
16	3-hydroxyisobutyrate dehydrogenase	Hibadh	Q99L13	66%/76	36.4	59.3	1.63	26.2	0.72	31.9	0.87	8.37/35.82	6.9/31.5
6	methylmalonate-semialdehyde/malonate-semialdehyde dehydrogenase [acylating]	Aldh6a1	Q9EQ20	64%/96	47.7	74.7	1.56	57.1	1.2	72.8	1.53	8.29/58.34	6.3/53.7
7	methylmalonate-semialdehyde dehydrogenase/malonate-semialdehyde dehydrogenase [acylating]	Aldh6a1	Q9EQ20	69%/107	226.5	171.2	0.76	167.5	0.74	182.1	0.8	8.29/58.34	6.1/50.5
17	3-hydroxyanthranilate 3,4-dioxygenase	Haao	Q78JT3	90%/106	58.8	77.1	1.31	76	1.29	83.1	1.41	5.54/28.75	7.6/31.4

Acc. no. – accession number in Uniprot database, Seq. cov. – sequence coverage, M. score – Mascot score, STD – control group fed standard diet, SFA – experimental group fed a high fat diet rich in saturated fatty acids, HR – experimental group fed a high fat diet with the linoleic acid/α-linolenic acid ratio 14:1, LR – experimental group fed a high fat diet with the linoleic acid/α-linolenic acid ratio of 5:1. Spot numbers (No.) correspond to those in Figure 1. The shading colours of the table represent downregulation (green) and upregulation (red) of protein expression. Colour intensity increases with higher down- or upregulation. White colour indicates a level of expression equal to the control group. Significant differences between the control and experimental group are marked in bold ($P \leq 0.05$)

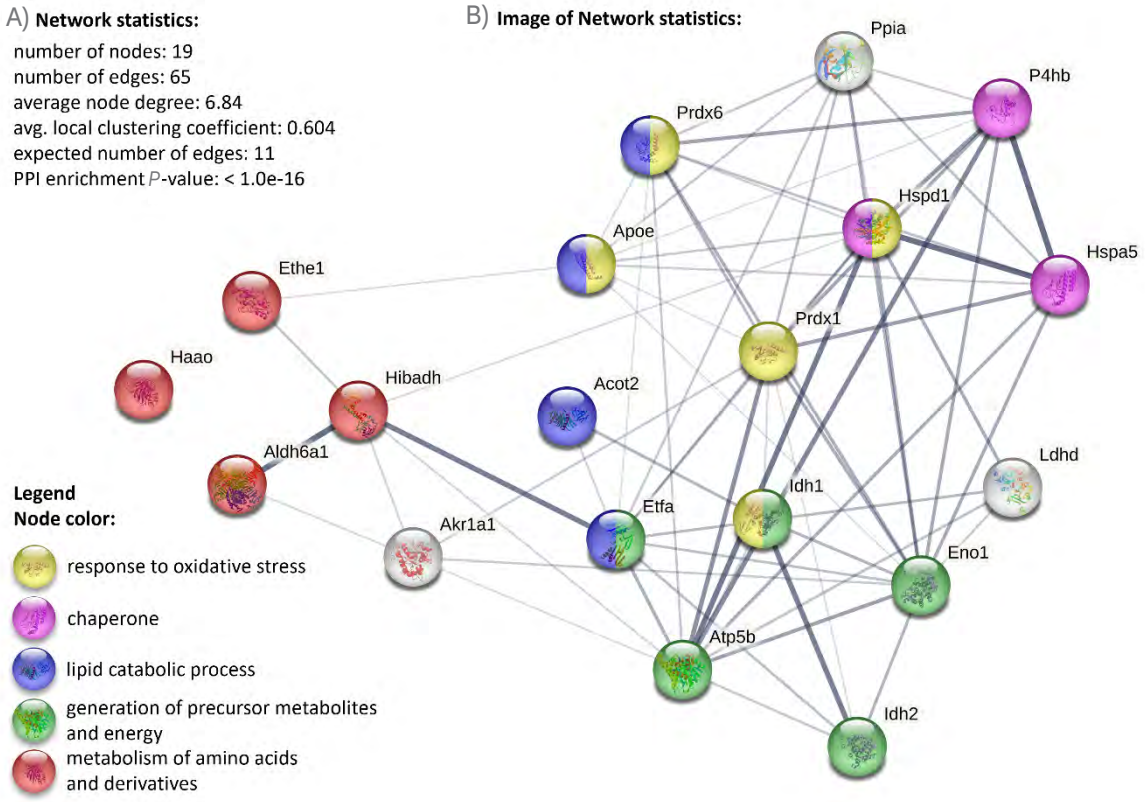

Figure 2. STRING analysis of identified gene expression: (A) protein-protein interaction image displaying nodes (gene products) and edges between all identified proteins affected by high-fat diets in mouse kidneys. Different edge thicknesses indicate the strength and nature of the depicted interactions detected between proteins. Different node colours show selected gene ontology (GO) terms, such as biological process, annotated keywords and local network cluster (STRING); (B) network statistics presenting data on the number of nodes and edges, average node degree, average local clustering coefficient, expected number of edges, and protein-protein interactions (PPI) enrichment *P*-value

Hspa5 – endoplasmic reticulum chaperone BiP, Hspd1 – 60 kDa heat shock protein, Prdx1 – peroxiredoxin 1, Prdx6 – peroxiredoxin 6, P4hb – protein-disulphide isomerase, Ppia – peptidyl-prolyl cis-trans isomerase A, Akr1a1 – aldo-keto reductase family 1 member A1, Eno1 – alpha-enolase, LDHD – probable D-lactate dehydrogenase, Acot2 – acyl-coenzyme A thioesterase 2, Ethe1 – persulphide dioxygenase ETHE1, ApoE – apolipoprotein E, Idh1 – isocitrate dehydrogenase [NADP] cytoplasmic, Idh2 – isocitrate dehydrogenase [NADP], mitochondrial, Etfa – electron transfer flavoprotein subunit alpha, Atp5f1b – ATP synthase subunit beta, Hibadh – 3-hydroxyisobutyrate dehydrogenase, Aldh6a1 – methylmalonate-semialdehyde/malonate-semialdehyde dehydrogenase [acylating], Haao – 3-hydroxyanthranilate 3,4-dioxygenase

Gene ontology analysis of differentially regulated proteins

To categorise proteins based on their involvement in known biological processes, a functional protein association analysis was conducted using the on-line bioinformatic software STRING v11.5. The enrichment showed a statistically significant association between 19 proteins differentially regulated by the consumed HFDs, with a protein-protein interaction (PPI) *P*-value equal to 1.0×10^{-16}. The functional PPI enrichment was carried out using the *Mus musculus domesticus* genome as the background. The analysis has revealed that differentially regulated proteins are involved in known biological processes and metabolic pathways, including generation of precursor metabolites and energy ($P = 0.0028$), lipid catabolic processes ($P = 0.017$), amino acid metabolism ($P = 0.0157$) and oxidative stress response ($P = 0.0066$). Additionally, several differentially expressed proteins were also classified as chaperones ($P = 0.0294$). The resulted PPI network, showing proteins as nodes and their known and predicted interactions as edges between proteins, is presented in Figure 2. The differentially regulated proteins were categorised into individual groups based on the enrichment analysis (Table 3).

Discussion

In the present study, we demonstrated that the consumption of HFDs induced changes in the expression pattern of proteins involved in various cellular processes, including energetic and amino acid metabolism, as well as cellular stress

prevention. These results are consistent with the findings of Dozio et al. (2022), who also reported changes in the expression of genes/proteins related to lipid metabolism, cellular stress response, and renal fibrosis development in mice fed HFDs. The present findings also align with our earlier observations, indicating that three months of feeding with HFDs differing in FA composition induced significant alterations in renal histological structure in mice. Specifically, animals receiving SFA and HR diets exhibited increased lipid vacuolisation in tubular epithelial cells, followed by an elevated number of apoptotic tubular cells, and higher collagen deposition in the renal interstitium. Those histological lesions were accompanied by increased expression of the *Kim1* gene, serving as a marker of tubular cell damage, as well as an upregulation of genes involved in oxidative stress prevention (Wypych et al., 2023). These observations are complemented by the results of the renal biochemistry profile obtained in the present study, revealing increased triglyceride accumulation in animals fed SFA and HR diets, as well as significantly higher TBARS levels in animals of the HR group. Furthermore, significantly lower plasma chloride ion concentrations were recorded in all experimental groups, which was most likely related to obesity. This observation is supported by the findings of Timerga and Haile (2021), who reported a correlation between the development of obesity and electrolyte imbalance leading to hypochloraemia.

Lipid metabolism-related proteins

Proximal tubule cells (PTCs) have a high energy demand due to their essential role in solute reabsorption and secretion from and into the tubular lumen. Thus, they require a high ATP production, which can only be ensured if the mitochondrial energetic metabolism is preserved. Mitochondrial FA β-oxidation (FAO) is the main source of intermediates for ATP synthesis in PTCs (Bhargava and Schnellmann, 2017). The increased dietary load of FA prompts cellular efforts to metabolise these energetic substrates through FAO. However, if FA supply exceeds mitochondrial β-oxidation capacity, the unmetabolised pool of FA is converted into triglycerides (TG) and stored in the form of intracellular lipid droplets (Tang et al., 2016). In the current study, an increased expression of ACOT2 protein was observed in the kidneys of animals fed the SFA diet. This enzyme belongs to the group of mitochondrial acyl-CoA thioesterases, i.e., proteins responsible for the hydrolysis of fatty acyl-CoAs to free fatty acids (FFA) and coenzyme-A. This process regulates the level of substrates available for mitochondrial fatty acid β-oxidation (Hunt and Alexson, 2002). Under conditions of excess FA supply, ACOT2 serves as a siphon that enables proximal tubule cells to maintain FAO in the mitochondria. This is due to the fact that other mitochondrial ACOTs are inhibited by high concentration of CoA, which can significantly reduce the efficiency of FAO (Bekeova et al., 2019). The observed overexpression of ACOT2 in the SFA group may be interpreted as an adaptive response facilitating the transfer of fatty acid metabolism from the peroxisome to the mitochondrion, thereby allowing efficient FA metabolism via the β-oxidation pathway. These findings align with the observations of Dozio et al. (2022), who also reported a significant decrease in the expression of peroxisomal proteins and an upregulation of ACOT2 both at the gene and protein levels in the kidney of mice fed an SFA-based HFD for 20 weeks.

The FA pool that cannot be metabolised via β-oxidation is converted into triglycerides and subsequently stored within lipid-containing vacuoles in tubular epithelial cells. According to Blue et al. (1983), the kidneys play a significant role in cholesterol and triglyceride metabolism, and thus require an efficient mechanism to eliminate surplus of these compounds. Additionally, an excess of FA can disrupt the reverse cholesterol and TG transport from the kidney through the apolipoprotein system (Pan, 2022). The increased accumulation of lipids in proximal tubule cells (PTC) can potentially induce lipotoxicity, cellular stress, and ultimately contribute to the onset of CKD (Sun et al., 2020). In our study, we observed a significant decrease in Apo-E levels, leading to increased deposition of triglycerides in the kidneys of animals fed the SFA diet. Reduced Apo-E expression is likely one of the factors responsible for impaired cellular lipid clearance, leading to the increased lipid vacuolisation and apoptosis rate observed in the kidneys of the SFA-fed group, as found in our previous study (Wypych et al., 2023). On the other hand, we observed an elevated expression of protein disulphide isomerase (PDI) in the kidneys of the LR group. Interestingly, in this group, we found only a limited number of lipid-containing vacuoles and low renal triglyceride content when compared to the control group. PDI is primarily recognised as an enzyme responsible for the formation and cleavage of disulphide bonds in newly synthesised proteins (Fu et al., 2021). However, in highly metabolically active tissues, PDI, as part of the P subunit, binds to the M subunit

to form microsomal triglyceride transfer protein (MTP) (Wetterau et al., 1991). MTP is expressed in renal proximal tubular epithelial cells and is required for the proper assembly of apolipoprotein B (Apo-B), which in turn contributes to TG secretion from kidney cells. Increased renal expression of this protein has been proposed as a preventive mechanism to mitigate the detrimental effects of elevated FA intake (Krzystanek et al., 2010). In our opinion, this mechanism was triggered in the kidneys of animals from the LR group, which, despite being fed an HFD, did not exhibit increased triglyceride accumulation and lipid vacuolisation. It should also be noted that despite the expected increase in cholesterol and TG efflux from the kidneys, animals in this group did not display any signs of dyslipidaemia (Liput et al.2021).

Proteins involved in the TCA cycle and respiratory electron transport chain (ETC)

The TCA cycle is mainly responsible for the synthesis of electron donors, the reduced form of nicotinamide adenine dinucleotide (NADH), and the reduced form of flavin adenine dinucleotide ($FADH_2$) to feed the ETC and maintain ATP synthesis. However, these intermediates also serve as signalling molecules to preserve cell functions, e.g., maintaining red-ox homeostasis (Jiménez-Uribe et al., 2021). In this study, we observed a significantly altered expression of two isoforms of isocitrate dehydrogenase (IDH1 and IDH2) in response to the administration of HFDs. Specifically, IDH1 expression was decreased in the SFA group, and in the LR group, three spots representing this protein were differentially regulated, with two being downregulated and one being upregulated. Conversely, IDH2 expression was significantly upregulated in the HR group. Both enzymes are responsible for the conversion of isocitrate into α-ketoglutarate, accompanied by the reduction of NADP+ (Jo et al., 2001). NADPH is known to be an important substrate for ROS detoxification, as it participates in glutathione regeneration and thioredoxin activity (Xiao et al., 2018). Moreover, α-ketoglutarate, despite being a necessary intermediate product in the TCA cycle, also acts as an H_2O_2 scavenger, serving as a non-enzymatic antioxidant (Bayliak et al., 2016). In light of this, IDH1 and IDH2 have been proposed as important NADPH producers in the cytoplasm and mitochondria, respectively, serving additionally as major antioxidant enzymes (Jo et al., 2001; Noh et al., 2020). It can be inferred that the decrease in IDH1 expression in the SFA group was related to perturbations in ROS detoxification processes in the kidneys. On the other hand, elevated IDH2 expression in the mitochondria in the HR group could be related to the activation of oxidative stress prevention mechanisms.

According to Ruggiero et al. (2011), in the kidneys of animals subjected to a short-term high-fat diet (HFD), despite the marked induction of cellular and subcellular oxidative stress caused by increased FAO, tubular cells developed an adaptive response to maintain respiratory function without stimulating mitochondrial biogenesis. However, Szeto et al. (2016) demonstrated that prolonged FFA overload, exceeding the capacity of the β-oxidation pathway, caused deposition of unmetabolised lipids in tissues, induction of lipotoxicity and impairment of ATP synthesis in mitochondrial electron transport chain as a consequence of oxidative stress induction. In the current study, a significant downregulation of the ATP synthase subunit beta was also observed in the kidneys of mice fed all HFDs. These results have confirmed that excessive FA supply reduces the efficiency of oxidative phosphorylation. On the other hand, enhanced expression of ETFA protein was found in the LR group. ETFA, together with the ETFB subunit, forms electron-transferring flavoprotein (ETF), a protein that links FAO and branched-chain amino acid oxidation to ETC. ETF is a specific electron acceptor for electron-transferring flavoprotein ubiquinone dehydrogenase, which drives coenzyme Q10 (CoQ10) (Henriques et al., 2021). Hence, the increased expression of ETFA1 could suggest the highest efficiency of β-oxidation in the LR group. These results are particularly interesting in light of the findings of Rombaldova et al. (2017), who demonstrated that n-3 PUFA supplementation could stimulate FAO in extrarenal cells. In the LR group, we also observed increased expression of ETHE1, an enzyme involved in the regulation of H_2S levels in cells. It is known that H_2S serves as a regulator of cellular energetic homeostasis (Paul et al., 2021). Its oxidation by sulphide quinone oxidoreductase (SQR) fuels ETC activity through CoQ10. SQR oxidises H_2S using glutathione (GSH) as an electron acceptor, converting it into GSSH, which is subsequently oxidised by ETHE1 protein to sulphite (Tiranti et al., 2009). The balance in the activity of enzymes involved in the synthesis and degradation of H_2S is crucial for maintaining their optimal levels in the mitochondria. Notably, a deficiency of H_2S can stimulate mitochondrial biogenesis, while an excess may inhibit the activity of complex IV of

ETC, diminishing the energy yield in the process of oxidative phosphorylation (OxPhos) (Paul et al., 2021). Thus, it can be speculated that the increased ETHE1 expression is closely related to the regulation of mitochondrial homeostasis in the LR group.

Glycolysis-related proteins

Metabolic reprogramming of the kidney is frequently a hallmark and a potential contributing factor to the development of kidney disease (Gewin, 2021). It has been proven that metabolic disorders, such as obesity and diabetes can significantly modify the energetic metabolism of kidney tubular cells (Linnan et al., 2021). Increased activity of key enzymes of the glycolytic pathway has previously been observed in the kidneys of genetically obese (ob/ob) mice compared to lean animals (Sochor et al., 1988). Furthermore, dyslipidaemia and hyperglycaemia, which often accompany diabetes, induce FA metabolism and glycolysis in the kidney to compensate for the loss of ATP in the TCA cycle (Sas et al., 2016). As mentioned previously, an HFD induces multiple alterations in energetic metabolism, leading to a decrease in ATP synthesis via the OxPhos pathway (Szeto et al., 2016). It can be speculated that a similar mechanism may exist in the kidneys of animals fed an SFA diet, where an elevated expression of LDHD and a simultaneous decrease in ATP synthase expression were observed. Furthermore, lactate synthesis as a result of a metabolic shift towards glycolysis was also observed in CKD development (Li et al., 2021). The SFA group exhibited the highest severity of pathophysiological lesions, potentially disrupting cellular metabolism, as reported in our previous study (Wypych et al., 2023).

Interestingly, increased expression of AKR1A1 protein was observed in the kidneys of animals fed both the LR and HR diets. This protein is involved in the glycolytic pathway; however, it shows pleiotropic effects. It has also been demonstrated that AKR1A1 participates in the detoxification of lipid peroxidation products (Burczynski et al., 2001), including reactive carbonyl species generated during PUFA autoxidation (Singh et al., 2015). The increased expression of AKR1A1 was consistent with the results of TBARS analysis, which revealed the highest degree of lipid peroxidation in the HR group. It should be noted that AKR1A1 also participates in the synthesis of L-ascorbic acid in mice, which is an antioxidant compound (Gabbay et al., 2010). Thus, it can be suspected that its increased expression may be induced by PUFA metabolites and may at least partially prevent oxidative stress in mouse kidneys.

Stress-related proteins

HFD modifies renal metabolism, leading to the generation of cellular stress. This forces cells to activate adaptive processes that eliminate the stressors and signalling pathways that may participate in tissue remodelling by promoting inflammation and fibrogenesis, ultimately leading to CKD (Gallazzini and Pallet, 2018). The increased ROS generation in metabolic processes, such as FAO, induce the expression of free radical scavengers in the kidneys of animals receiving HFDs. Moreover, a high ROS level also leads to the development of endoplasmic reticulum stress, leading to changes in the expression of molecular chaperones. In the present study, we observed symptoms of oxidative stress in the kidneys of animals fed HR and SFA diets, manifested by increased TBARS values. Moreover, feeding HFDs modified the expression of two important ROS scavengers, namely PRDX6 and PRDX1. The key function of PRDX6 is the detoxification of cells from excess H_2O_2 and lipid hydroperoxides. However, this protein may also be involved in promoting FAO in animals fed HFDs (Arriga et al., 2019). In our study, this protein was represented by two spots that differed in pI distribution. These pI shifts could reflect post-translational modifications of this protein related to its antioxidative function, such as S-oxidation, S-glutathionylation, and sulphonylation, which may alter the protein's activity (Jeong et al., 2012). Consequently, the modification of the expression pattern of this protein in the animals from the SFA and HR groups could indicate the induction and exacerbation of oxidative stress or be related to the regulation of the FAO process in the kidneys of those animals. On the other hand, PRDX1 expression was increased in the kidneys of animals fed the SFA and LR diets. This protein primarily regulates H_2O_2 scavenging, however, it may also exhibit chaperone activity (Neumann et al., 2009). Similarly to PRDX6, the induction of PRDX1 expression may reflect the intensity of cellular ROS generation (Mei et al., 2015). It should be emphasised that PRDX1 activity is regulated by thioredoxins, thioreductases, and NADPH (Neumann et al., 2009), offering partial explanation for the increased expression of PDI in the LR group. While PDI primarily functions as a chaperonin, it also has thioredoxin-like properties and interacts with over-oxidised PRDX1 to restore its ROS scavenger function (Soares Moretti and

Martins Laurindo, 2017). In our previous report, we also observed an increased expression of ROS scavengers, SOD and CAT, at the gene level in the kidneys of mice fed the HR diet. Despite the confirmed induction of oxidative stress in the kidneys of this group of animals, we did not observe increased activity of these enzymes in that organ. A similar phenomenon was described by Omar et al. (1999), who observed induced expression of ROS scavenger genes but reduced enzyme activities during the development of extrarenal degenerative disease. We have also observed enhanced expression of PPIA protein in the kidneys of animals from the SFA and HR groups. Its expression is induced by cellular stressors. Under oxidative stress conditions, PPIA undergoes oxidation, stimulating the secretion of this protein into the extracellular fluid (Soe et al., 2014). As an intracellular protein, PPIA serves as a weak chaperonin, but as a secreted protein, it is a potent regulator of inflammation and apoptosis in epithelial cells (Xue et al., 2017; Cabello et al., 2021). Therefore, the increased expression of PPIA in the kidneys of mice fed SFA and HR diets may be associated with a higher rate of apoptosis observed in these animals (Wypych et al., 2023). The results of the current study also demonstrated a decreased expression of two chaperones, namely HSPA5 and HSPD1, in the kidneys of the HR- and SFA-fed animals, respectively. This phenomenon is difficult to explain in light of the significant induction of endoplasmic reticulum stress caused by the administration of HFDs recorded in other studies (Xie et al., 2016; Sánchez-Navarro et al., 2021).

Amino acid metabolism-related proteins

The kidney is a key organ involved in amino acid metabolism, filtering over 50 g of AA per day in the glomeruli, with the majority being reabsorbed in the proximal tubules (Verrey et al., 2005). A portion of the reabsorbed amino acids can be utilised as substrates for gluconeogenesis. Moreover, branched-chain amino acids can serve as an energy source, undergoing oxidation in various points of the tricarboxylic acid (TCA) cycle (Neinast et al., 2019). Both obesity and HFD feeding are factors that may affect amino acids metabolism in the kidney (Mantha et al., 2018). It has been previously shown that HFDs may shift epithelial cell metabolism to amino acid catabolism (Mantha et al., 2018). On the other hand, metabolic disorders, such as metabolic syndrome and type 2 diabetes can cause significant disturbances in amino acid metabolic homeostasis (Zhu et al., 2022). In the present study, an increased expression of two enzymes was observed, HIBADH and ALDH6A1, which participate in the degradation of one of the intermediates of valine catabolism – 3-hydroxyisobutyrate (3-HIB) – in the kidneys of mice fed an SFA diet. This peptide serves as a precursor for succinyl-CoA and may serve as a substrate in *de novo* FA synthesis. The HIBADH knock-out in rats was shown to stimulate cellular FA intake (Jang et al., 2016). However, it should be pointed out that the expression of HIBADH was significantly reduced in the kidneys of genetically obese male mice, exhibiting symptoms of metabolic syndrome (Dominguez et al., 2006). This may suggest that the increased expression of enzymes involved in 3-HIB degradation, observed in the SFA group, could serve as a regulatory mechanism of cellular FA uptake. Interestingly, the expression of ALDH6A1 was decreased in the kidneys of mice fed the HR diet, a phenomenon that warrants further investigation. Additionally, our study found an overexpression of HAAO protein in the kidneys of mice fed the LR diet. HAAO is an enzyme participating in the tryptophan-kynurenine pathway, and it also converts 3-hydroxyanthranilic acid to quinolinic acid, thereby promoting NAD+ bioavailability (Shi et al., 2017). This nucleotide is a hub electron carrier that is involved in numerous metabolic processes. Defective NAD+ synthesis contributes to the development of kidney diseases, while maintaining NAD+ bioavailability may mitigate long-term profibrotic pathways leading to CKD (Ralto et al., 2020). Previous studies have shown that n-3 fatty acids may stimulate NAD+ biosynthesis in extrarenal tissues (Chi et al., 2022). Therefore, it is plausible that the high ALA levels in the LR diet could be responsible for attenuating fibrotic changes observed in the SFA and HR groups.

Conclusions

It can be concluded that the protein expression profile of the kidney varied depending on the qualitative fatty acids (FA) composition of a high-fat diet (HFD). Feeding HFDs affected the expression pattern of proteins involved in energetic metabolism (FA β-oxidation, glycolysis, tricarboxylic acid cycle, and oxidative phosphorylation), amino acid catabolism, and cellular stress prevention.

The expression pattern of proteins related to energetic metabolism was most significantly affected by the administration of an HFD rich in SFA. The ingestion of an HFD rich in omega 6 PUFA and SFA contributed to oxidative stress in mouse kidneys and

caused downregulation of molecular chaperones and subsequent induction of proteins engaged in the regulation of inflammation and apoptosis.

Funding

This work was financially supported by two sources. The dietary experiment was carried out with the support of the KNOW (Leading National Research Centre) Scientific Consortium 'Healthy Animal – Safe Food' under the decision of the Ministry of Science and Higher Education No. 05-1/KNOW2/2015, grant No. KNOW2015/CB/PRO1/44. The analyses performed were supported by the Rector of the West Pomeranian University of Technology in Szczecin for PhD students of the Doctoral School, grant number: 35/2022.

Conflict of interest

The Authors declare that there is no conflict of interest.

References

Arriga R., Pacifici F., Capuani B. et al., 2019. Peroxiredoxin 6 is a key antioxidant enzyme in modulating the link between glycemic and lipogenic metabolism. Oxid. Med. Cell. Longev. 2019, 9685607, https://doi.org/10.1155/2019/9685607

Bayliak M.M., Lylyk M.P., Vytvytska O.M., Lushchak V.I., 2016. Assessment of antioxidant properties of alpha-keto acids in vitro and in vivo. Eur. Food Res. Technol. 242, 179–188, https://doi.org/10.1007/s00217-015-2529-4

Bekeova C., Anderson-Pullinger L., Boye K., Boos F., Sharpadskaya Y., Herrmann J.M., Seifert E.L., 2019. Multiple mitochondrial thioesterases have distinct tissue and substrate specificity and CoA regulation, suggesting unique functional roles. J. Biol. Chem. 294, 19034–19047, https://doi.org/10.1074/jbc.RA119.010901

Bhargava P., Schnellmann R.G., 2017. Mitochondrial energetics in the kidney. Nat. Rev. Nephrol. 13, 629–646, https://doi.org/10.1038/nrneph.2017.107

Blue M.L., Williams D.L., Zucker S., Khan S.A., Blum C.B., 1983. Apolipoprotein E synthesis in human kidney, adrenal gland, and liver. Proc. Natl. Acad. Sci. USA 80, 283–287, https://doi.org/10.1073/pnas.80.1.283

Burczynski M.E., Sridhar G.R., Palackal N.T., Penning T.M., 2001. The reactive oxygen species- and michael acceptor-inducible human aldo-keto reductase AKR1C1 reduces the α,β-unsaturated aldehyde 4-hydroxy-2-nonenal to 1,4-dihydroxy-2-nonene. J. Biol. Chem. 276, 2890–2897, https://doi.org/10.1074/jbc.M006655200

Cabello R., Fontecha-Barriuso M., Martin-Sanchez D., Lopez-Diaz A.M., Carrasco S., Mahillo I., Gonzalez-Enguita C., Sanchez-Nino M.D., Ortiz A., Sanz A.B., 2021. Urinary cyclophilin a as marker of tubular cell death and kidney injury. Biomedicines 9, 1–19, https://doi.org/10.3390/biomedicines9020217

Chi D.H., Kahyo T., Islam A. et al., 2022. NAD+ levels are augmented in aortic tissue of ApoE-/-mice by dietary omega-3 fatty acids. Arterioscler. Thromb. Vasc. Biol. 42, 395–406, https://doi.org/10.1161/ATVBAHA.121.317166

Chodkowska K.A., Abramowicz-Pindor P.A., Tuśnio A., Gawin K., Taciak M., Barszcz M., 2022. Effect of phytobiotic composition on production parameters, oxidative stress markers and myokine levels in blood and pectoral muscle of broiler chickens. Animals 12, 2625, https://doi.org/10.3390/ani12192625

Dominguez J.H., Wu P., Hawes J.W., Deeg M., Walsh J., Packer S.C., Nagase M., Temm C., Goss E., Peterson R., 2006. Renal injury: Similarities and differences in male and female rats with the metabolic syndrome. Kidney Int. 69, 1969–1976, https://doi.org/10.1038/sj.ki.5000406

Dozio E., Maffioli E., Vianello E., Nonnis S., Scalvini F.G., Spatola L., Roccabianca P., Tedeschi G., Romanelli M.M.C., 2022. A wide-proteome analysis to identify molecular pathways involved in kidney response to high-fat diet in mice. Int. J. Mol. Sci. 23, 3809, https://doi.org/10.3390/ijms23073809

Fu J., Gao J., Liang Z., Yang D., 2021. PDI-regulated disulfide bond formation in protein folding and biomolecular assembly. Molecules 26, 171, https://doi.org/10.3390/molecules26010171

Gabbay K.H., Bohren K.M., Morello R., Bertin,T., Liu J., Vogel P., 2010. Ascorbate synthesis pathway: Dual role of ascorbate in bone homeostasis. J. Biol. Chem. 285, 19510–19520, https://doi.org/10.1074/jbc.M110.110247

Gallazzini M., Pallet N., 2018. Endoplasmic reticulum stress and kidney dysfunction. Biol. Cell. 110, 205–216, https://doi.org/10.1111/boc.201800019

Gewin L.S., 2021. Sugar or fat? Renal tubular metabolism reviewed in health and disease. Nutrients 13, 1580, https://doi.org/10.3390/nu13051580

Henriques B.J., Olsen R.K.J., Gomes C.M., Bross, P., 2021. Electron transfer flavoprotein and its role in mitochondrial energy metabolism in health and disease. Gene 776, 145407, https://doi.org/10.1016/j.gene.2021.145407

Herosimczyk A., Lepczyński A., Werkowska M. et al., 2022. Dietary inclusion of dried chicory root affects cecal mucosa proteome of nursery pigs. Animals 12, 1710, https://doi.org/10.3390/ani12131710

Hunt M.C., Alexson S.E.H., 2002. The role Acyl-CoA thioesterases play in mediating intracellular lipid metabolism. Prog. Lipid Res. 41, 99–130, https://doi.org/10.1016/S0163-7827(01)00017-0

Jang C., Oh S.F., Wada S., et al., 2016. A branched-chain amino acid metabolite drives vascular fatty acid transport and causes insulin resistance. Nat. Med. 22, 421–426, https://doi.org/10.1038/nm.4057

Jeong J., Kim Y., Kyung Seong J., Lee K.J., 2012. Comprehensive identification of novel post-translational modifications in cellular peroxiredoxin 6. Proteomics 12, 1452–1462, https://doi.org/10.1002/pmic.201100558

Jiménez-Uribe A.P., Hernández-Cruz E.Y., Ramírez-Magaña K.J., Pedraza-Chaverri J., 2021. Involvement of tricarboxylic acid cycle metabolites in kidney diseases. Biomolecules 11, 1259, https://doi.org/10.3390/biom11091259

Jo S.H., Son M.K., Koh, H.J. et al., 2001. Control of mitochondrial redox balance and cellular defense against oxidative damage by mitochondrial NADP+-dependent isocitrate dehydrogenase. J. Biol. Chem. 276, 16168–16176, https://doi.org/10.1074/jbc.M010120200

Krzystanek M., Pedersen T.X., Bartels E.D., Kjaehr J., Straarup E.M., Nielsen L.B., 2010. Expression of apolipoprotein B in the kidney attenuates renal lipid accumulation. J. Biol. Chem. 285, 10583–10590, https://doi.org/10.1074/jbc.M109.078006

Lepczyński A., Ożgo M., Michałek K., Dratwa-Chałupnik A., Grabowska M., Herosimczyk A., Liput K.P., Poławska E., Kram A., Pierzchała M., 2021. Effects of three-month feeding high fat diets with different fatty acid composition on myocardial proteome in mice. Nutrients 13, 330, https://doi.org/10.3390/nu13020330

Li Y., Sha Z., Peng H., 2021. Metabolic reprogramming in kidney diseases: Evidence and therapeutic opportunities. Int. J. Nephrol. 2021, 5497346, https://doi.org/10.1155/2021/5497346

Linnan B., Yanzhe W., Ling Z., Yuyuan L., Sijia C., Xinmiao X., Fengqin L., Xiaoxia W., 2021. *In situ* metabolomics of metabolic reprogramming involved in a mouse model of type 2 diabetic kidney disease. Front. Physio. 12, 779683, https://doi.org/10.3389/fphys.2021.779683

Liput K.P., Lepczyński A., Ogłuszka M., Nawrocka A., Poławska E., Grzesiak A., Ślaska B., Pareek C.S., Czarnik U., Pierzchała M., 2021. Effects of dietary n-3 and n-6 polyunsaturated fatty acids in inflammation and cancerogenesis. Int. J. Mol. Sci. 22, 6965, https://doi.org/10.3390/ijms22136965

Liput K.P., Lepczyński A., Nawrocka A. et al., 2021. Effects of three-month administration of high-saturated fat diet and high-polyunsaturated fat diets with different linoleic acid (LA, C18:2n-6) to α-linolenic acid (ALA, C18:3n-3) ratio on the mouse liver proteome. Nutrients 13, 1678, https://doi.org/10.3390/nu13051678

Mantha O.L., Polakof S., Huneau J.F., Mariotti F., Poupin N., Zalko D., Fouillet H., 2018. Early changes in tissue amino acid metabolism and nutrient routing in rats fed a high-fat diet: Evidence from natural isotope abundances of nitrogen and carbon in tissue proteins. Br. J. Nut. 119, 981–991, https://doi.org/10.1017/S0007114518000326

Marklund S., Marklund G., 1974. Involvement of the superoxide anion radical in the autoxidation of pyrogallol and a convenient assay for superoxide dismutase. Eur. J. Biochem. 47, 469–474, https://doi.org/10.1111/j.1432-1033.1974.tb03714.x

Mei W., Peng Z., Lu M. et al., 2015. Peroxiredoxin 1 inhibits the oxidative stress induced apoptosis in renal tubulointerstitial fibrosis. Nephrology 20, 832–842, https://doi.org/10.1111/nep.12515

Neinast M.D., Jang C., Hui S. et al., 2019. Quantitative analysis of the whole-body metabolic fate of branched-chain amino acids. Cell Metab. 29, 417–429, https://doi.org/10.1016/j.cmet.2018.10.013

Neumann C.A., Cao J., Manevich Y., 2009. Peroxiredoxin 1 and its role in cell signaling. Cell Cycle 8, 4072–4078, https://doi.org/10.4161/cc.8.24.10242

Noh M.R., Kong M.J., Han S.J., Kim J.I., Park K.M., 2020. Isocitrate dehydrogenase 2 deficiency aggravates prolonged high-fat diet intake-induced hypertension. Redox Biol. 34, 101548, https://doi.org/10.1016/j.redox.2020.101548

Omar R.A., Chyan Y.-J., Andorn A.C., Poeggeler B., Robakis N.K., Pappolla M.A., 1999. Increased expression but reduced activity of antioxidant enzymes in Alzheimer's disease. J. Alzheimer's Dis. 1, 139–145, https://doi.org/10.3233/JAD-1999-1301

Ong K.L., Marklund M., Huang L. et al., 2023. Association of omega 3 polyunsaturated fatty acids with incident chronic kidney disease: pooled analysis of 19 cohorts. B. Med. J. 380, e072909, https://doi.org/10.1136/bmj-2022-072909

Ożgo M., Lepczynski A., Herosimczyk A., 2015. Two-dimensional gel-based serum protein profile of growing piglets. Turk. J. Biol. 39, 320–327, https://doi.org/10.3906/biy-1408-45

Ożgo M., Skrzypczak W.F., Herosimczyk A., Mazur A., 2007. Proteomics in relation to renal physiology and pathophysiology. Med. Wet. 63, 1146–1150

Pan X., 2022. The roles of fatty acids and apolipoproteins in the kidneys. Metabolites 12, 462, https://doi.org/10.3390/metabo12050462

Paul B.D., Snyder S.H., Kashfi K., 2021. Effects of hydrogen sulfide on mitochondrial function and cellular bioenergetics. Redox Biol. 38, 101772, https://doi.org/10.1016/j.redox.2020.101772

Provenzano M., Serra R., Garofalo C. et al., 2022. OMICS in chronic kidney disease: Focus on prognosis and prediction. Int. J. Mol. Sci. 23, 336, https://doi.org/10.3390/ijms23010336

Ralto K.M., Rhee E.P., Parikh S.M., 2020. NAD^+ homeostasis in renal health and disease. Nat. Rev. Nephrol. 16, 99–111, https://doi.org/10.1038/s41581-019-0216-6

Rombaldova M., Janovska P., Kopecky J., Kuda O., 2017. Omega-3 fatty acids promote fatty acid utilization and production of pro-resolving lipid mediators in alternatively activated adipose tissue macrophages. Biochem. Biophys. Res. Commun. 490, 1080–1085, https://doi.org/10.1016/j.bbrc.2017.06.170

Ruggiero C., Ehrenshaft M., Cleland E., Stadler K., 2011. High-fat diet induces an initial adaptation of mitochondrial bioenergetics in the kidney despite evident oxidative stress and mitochondrial ROS production. Am. J. Physiol. Endocrinol. Metab. 300, E1047–E1058, https://doi.org/10.1152/ajpendo.00666.2010

Sánchez-Navarro A., Martínez-Rojas M.Á., Caldiño-Bohn R.I., Pérez-Villalva R., Zambrano E., Castro-Rodríguez, D.C., Bobadilla N.A., 2021. Early triggers of moderately high-fat diet-induced kidney damage. Physiol. Rep. 9, e14937, https://doi.org/10.14814/phy2.14937

Sas K.M., Kayampilly P., Byun J. et al., 2016. Tissue-specific metabolic reprogramming drives nutrient flux in diabetic complications. JCI Insight. 1, e86976, https://doi.org/10.1172/jci.insight.86976

Shi H., Enriquez A., Rapadas M. et al., 2017. NAD deficiency, congenital malformations, and niacin supplementation. N. Engl. J. Med. 377, 544–552, https://doi.org/10.1056/nejmoa1616361

Singh M., Kapoor A., Bhatnagar A., 2015. Oxidative and reductive metabolism of lipid-peroxidation derived carbonyls. Chem. Biol. Interact. 234, 261–273, https://doi.org/10.1016/j.cbi.2014.12.028

Soares Moretti A.I., Martins Laurindo F.R., 2017. Protein disulfide isomerases: Redox connections in and out of the endoplasmic reticulum. Arch. Biochem. Biophys. 617, 106–119, https://doi.org/10.1016/j.abb.2016.11.007

Sochor M., Kunjara S., McLean P., 1988. Regulation of pathways of glucose metabolism in the kidney. The activity of the pentose phosphate pathway, glycolytic route and the regulation of phosphofructokinase in the kidney of lean and genetically obese (ob/ob) mice; comparison with effects of diab. Horm. Metab. Res. 20, 676–681, https://doi.org/10.1055/s-2007-1010915

Soe N.N., Sowden M., Baskaran P., Kim Y., Nigro P., Smolock E.M., Berk B.C., 2014. Acetylation of cyclophilin A is required for its secretion and vascular cell activation. Cardiovasc. Res. 101, 444–453, https://doi.org/10.1093/cvr/cvt268

Sun Y., Ge X., Li X. et al., 2020. High-fat diet promotes renal injury by inducing oxidative stress and mitochondrial dysfunction. Cell Death Dis. 11, 914, https://doi.org/10.1038/s41419-020-03122-4

Syren M.L., Turolo S., Marangoni F., Milani G.P., Edefonti A., Montini G., Agostoni C., 2018. The polyunsaturated fatty acid balance in kidney health and disease: A review. Clin. Nutr. 37, 1829–1839, https://doi.org/10.1016/j.clnu.2017.11.019

Szeto H.H., Liu S., Soong Y., Alam N., Prusky G.T., Seshan S.V., 2016. Protection of mitochondria prevents high-fat diet-induced glomerulopathy and proximal tubular injury. Kidney Int. 90, 997–1011, https://doi.org/10.1016/j.kint.2016.06.013

Szklarczyk D., Kirsch R., Koutrouli M. et al., 2023. The STRING database in 2023: protein–protein association networks and functional enrichment analyses for any sequenced genome of interest. Nucleic Acids Res. 51, D638–D646, https://doi.org/10.1093/nar/gkac1000

Tang C., Cai J., Dong Z., 2016. Mitochondrial dysfunction in obesity-related kidney disease: a novel therapeutic target. Kidney Int. 90, 930-933, https://doi.org/10.1016/j.kint.2016.07.045

Than W.H., Chan G.C.-K., Ng J.K.-C., Szeto C.-C., 2020. The role of obesity on chronic kidney disease development, progression, and cardiovascular complications. Adv. Biomark. Sci. Technol. 2, 24–34, https://doi.org/10.1016/j.abst.2020.09.001

Timerga A., Haile K., 2021. Patterns of calcium- and chloride-ion disorders and predictors among obese outpatient adults in southern ethiopia. Diabetes Metab. Syndr. Obes. 14, 1349–1358, https://doi.org/10.2147/DMSO.S300434

Tiranti V., Viscomi C., Hildebrandt T. et al., 2009. Loss of ETHE1, a mitochondrial dioxygenase, causes fatal sulfide toxicity in ethylmalonic encephalopathy. Nat. Med. 15, 200–205, https://doi.org/10.1038/nm.1907

Verrey F., Ristic Z., Romeo E., Ramadan T., Makrides V., Dave M.H., Wagner C.A., Camargo S.M.R., 2005. Novel renal amino acid transporters. Annu. Rev. Physiol. 67, 557–572, https://doi.org/10.1146/annurev.physiol.67.031103.153949

Wetterau J.R., Aggerbeck L.P., Laplaud P.M., McLean L.R., 1991. Structural properties of the microsomal triglyceride-transfer protein complex. Biochem. 30, 4406-4412, https://doi.org/10.1021/bi00232a006

Wu F., Mao L., Zhang Y., Chen X., Zhuang P., Wang W., Wang J., Jiao J., 2022. Individual SFA intake and risk of overweight/obesity: Findings from a population-based nationwide cohort study. Br. J. Nutr. 128, 75–83, https://doi.org/doi:10.1017/S0007114521002890

Wypych A., Dunisławska A., Grabowska M., Michałek K., Ożgo M., Liput K., Herosimczyk A., Poławska E., Pierzchała M., Lepczyński A., 2023. Effects of three-month feeding high-fat diets with different fatty acid composition on kidney histology and expression of genes related to cellular stress and water-electrolyte homeostasis in mice. J. Anim. Feed Sci. 32, 372-384, https://doi.org/10.22358/jafs/163179/2023

Xiao W., Wang R.S., Handy D.E., Loscalzo J., 2018. NAD(H) and NADP(H) redox couples and cellular energy metabolism. Antioxid. Redox Signal. 28, 251–272, https://doi.org/10.1089/ars.2017.7216

Xie H., Huang L., Li Y., Zhang H., Liu H., 2016. Endoplasmic reticulum stress and renal lesion in mice with combination of high-fat diet and streptozotocin-induced diabetes. Acta Cir. Bras. 31, 150–155, https://doi.org/10.1590/S0102-865020160030000001

Xue C., Sowden M., Berk B.C., 2017. Extracellular cyclophilin A, especially acetylated, causes pulmonary hypertension by stimulating endothelial apoptosis, redox stress, and inflammation. Arterioscler. Thromb. Vasc. Biol. 37, 1138–1146, https://doi.org/10.1161/ATVBAHA.117.309212

Yang P., Xiao Y., Luo X., Zhao Y., Zhao L., Wang Y., Wu T., Wei L., Chen Y., 2017. Inflammatory stress promotes the development of obesity-related chronic kidney disease via CD36 in mice. J. Lipid Res. 58, 1417–1427, https://doi.org/10.1194/jlr.M076216

Zhu H., Bai M., Xie X., Wang J., Weng C., Dai H., Chen J., Han F., Lin W., 2022. Impaired amino acid metabolism and its correlation with diabetic kidney disease progression in type 2 diabetes mellitus. Nutrients 14, 3345, https://doi.org/10.3390/nu14163345